

# New Pyrazine Conjugates: Synthesis, Computational Studies, and Antiviral Properties against SARS-CoV-2

Israa A. Seliem,<sup>[a, b]</sup> Adel S. Girgis,<sup>[c]</sup> Yassmin Moatasim,<sup>[d]</sup> Ahmed Kandeil,<sup>[d]</sup> Ahmed Mostafa,<sup>[d]</sup> Mohamed A. Ali,<sup>[d]</sup> Mohamed S. Bekheit,<sup>[c]</sup> and Siva S. Panda\*<sup>[a]</sup>

Currently, limited therapeutic options are available for severe acute respiratory syndrome coronavirus-2 (SARS-CoV-2). We have developed a set of pyrazine-based small molecules. A series of pyrazine conjugates was synthesized by microwave-assisted click chemistry and benzotriazole chemistry. All the synthesized conjugates were screened against the SARS-CoV-2 virus and their cytotoxicity was determined. Computational

studies were carried out to validate the biological data. Some of the pyrazine-triazole conjugates (**5 d–g**) and (*S*)-*N*-(1-(benzo[*d*]thiazol-2-yl)-2-phenylethyl)pyrazine-2-carboxamide **12 i** show significant potency against SARS-CoV-2 among the synthesized conjugates. The selectivity index (SI) of potent conjugates indicates significant efficacy compared to the reference drug (Favipiravir).

## Introduction

An unknown viral infection originated from China in December 2019 and rapidly spread across the world.<sup>[1–3]</sup> The World Health Organization (WHO) identified the virus as the severe acute respiratory syndrome coronavirus-2 (SARS-CoV-2) on Feb. 11, 2020 and named it coronavirus disease 2019 (COVID-19). In March 2020, WHO declared the coronavirus outbreak as a global pandemic.<sup>[4]</sup> As of July 2021, over 200 million people have been infected, and more than 4.2 million people worldwide have died from the coronavirus. Although the world has survived numerous pandemics in the past, COVID-19 is an unprecedented global health challenge that has greatly impacted our lives and the socioeconomic structure of the world.

Very few antiviral drugs are available for the treatment of COVID-19 and most of them are ineffective. Of the few vaccines that were given emergency approval by the FDA, some are showing adverse side effects. The pandemic has spurred research into the development of new drugs and exploration of the existing antiviral drugs against COVID-19. By using efficient drug development to control the global pandemic and reducing the time from synthesis to FDA approval, the drug

repurposing approach would be the most accessible and pragmatic pathway. Many drugs were considered for this subject. Favipiravir is a drug that exhibits promising response with limitations such as cardiovascular, endocrine, gastrointestinal, and hepatic toxicity. As such, that drug may need further investigational studies (Figure 1).<sup>[5,6]</sup> Recently, several countries approved Favipiravir for emergency use to control the pandemic. As of April 2021; there are 33 studies registered on clinicaltrials.gov to assess the utilization of this drug in the management of COVID-19.<sup>[7]</sup>

New drug development process is challenging, time-consuming and expensive. Among various rational drug design strategies, molecular hybridization of bioactive moieties is a powerful and attractive approach because of several advantages such as a) increasing desired pharmacological activity; b) allowing for better selectivity towards the target; c) improving interaction with multiple pharmacological sites and d) decreasing possible cytotoxicity. Our continuous research mission is to actively design and develop potential drug candidates for targeted diseases by this molecular hybridization approach.<sup>[8–13]</sup>

Recently, we have reported a set of quinoline-triazole conjugates and some of them are showing promising activity against SARS-CoV-2.<sup>[14]</sup> In continuation of our drug development approach, we have utilized “click” chemistry” and “benzotriazole chemistry” in synthesizing new pyrazine-based conjugates as

[a] Dr. I. A. Seliem, Dr. S. S. Panda  
Department of Chemistry and Physics  
Augusta University, Augusta, GA 30912 (USA)  
E-mail: sipanda@augusya.edu  
sspanda12@gmail.com

[b] Dr. I. A. Seliem  
Department of Pharmaceutical Organic Chemistry, Faculty of Pharmacy  
Zagazig University, Zagazig 44519 (Egypt)

[c] Prof. A. S. Girgis, Dr. M. S. Bekheit  
Department of Pesticide Chemistry  
National Research Centre  
Dokki, Giza, 12622 (Egypt)

[d] Dr. Y. Moatasim, Dr. A. Kandeil, Dr. A. Mostafa, Prof. M. A. Ali  
Center of Scientific Excellence for Influenza Viruses  
National Research Centre  
Dokki, Giza, 12622 (Egypt)

Supporting information for this article is available on the WWW under <https://doi.org/10.1002/cmdc.202100476>

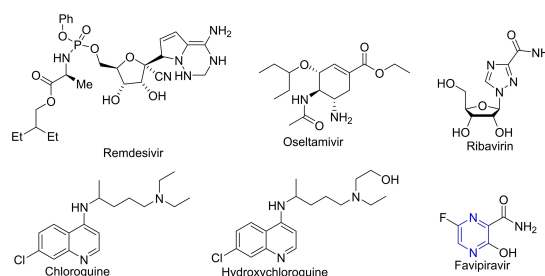
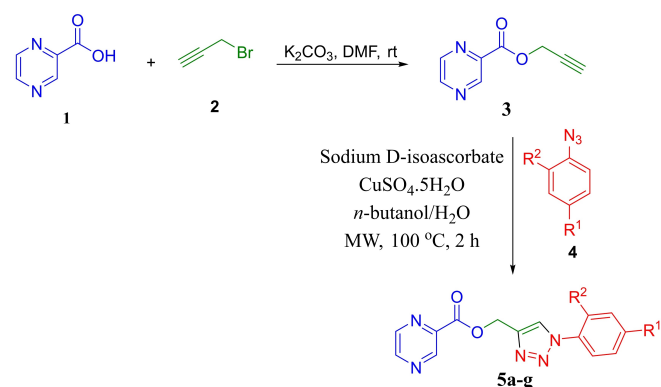


Figure 1. Examples of repurposing drugs for COVID19.

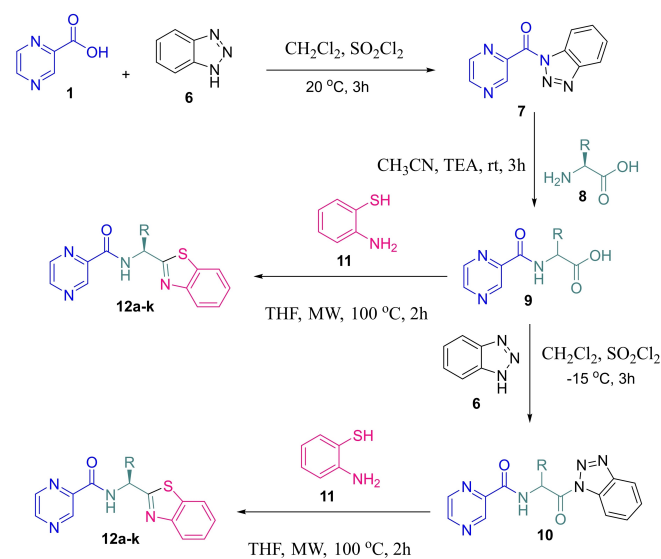
potential antiviral drug candidates for SARS-CoV-2. We have also synthesized another set of hybrid conjugate of pyrazine and benzothiazole using amino acids as linkers. We selected the pyrazine scaffold from the repurposing drug (Favipiravir) and triazole moiety because of their importance in the drug development process and because they are well-known for diversified biological properties.<sup>[15–19]</sup> Benzothiazole is also known for distinct biological properties including antitumor,<sup>[20]</sup> anti-inflammatory,<sup>[21]</sup> antimicrobial,<sup>[22]</sup> antitrypanosomal<sup>[23]</sup> anticonvulsant,<sup>[24]</sup> and antituberculosis<sup>[25]</sup> activities.

## Results and Discussion

An efficient strategy was developed to synthesize the desired pyrazine-triazole conjugates **5a–g** from pyrazine-based alkyne **3** with substituted aromatic azides **4** by adopting the well-established Cu-mediated click chemistry (Scheme 1). The precursor alkynes **3** were synthesized by treating a solution of



**Scheme 1.** Synthesis of pyrazine-triazole conjugates **5a–g**.



**Scheme 2.** Synthesis of pyrazine-benzothiazole conjugates **12a–k** with amino acid linkers.

pyrazinoic acid **1** in DMF with propargyl bromide (**2**) to obtain the alkyne component under the basic environment of potassium carbonate ( $K_2CO_3$ ) at room temperature. The azides of aromatic amines **4a–g** were synthesized following the previously reported procedure.<sup>[13]</sup>

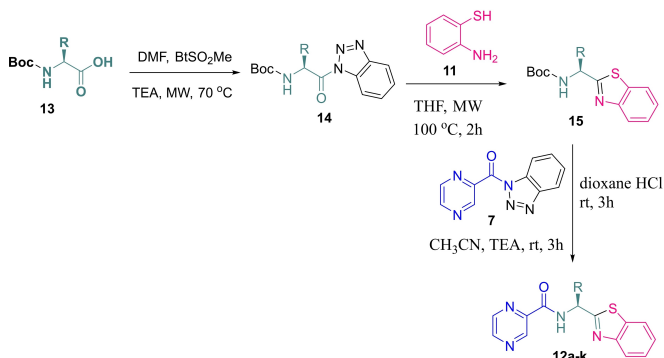
To diversify the pool of favipiravir-based compounds, we activated the carboxylic acid of pyrazinoic acid with benzotriazole and the benzotriazolide treated with various amino acids to get the pyrazinoic acid-amino acid conjugates. The conjugates were further treated with 2-amino thiophenol under microwave irradiation to obtain another set of conjugates **12a–k** containing pyrazine and benzothiazole moieties. We have also tried to synthesize the same set of conjugates **12a–k** using benzotriazole chemistry and in both routes, we observed similar results (Scheme 2).

We investigate an alternate route to synthesize the conjugates **12a–k** using Boc chemistry and benzotriazole chemistry to avoid the use of excessive thionyl chloride by following the synthetic route described in Scheme 3. In this route, we observed that the overall yield is lower than the previous route.

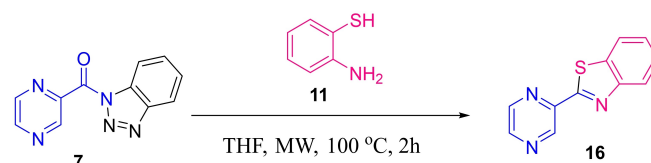
To understand the role of amino acids in the conjugates, we have synthesized the conjugate containing pyrazine and benzothiazole without amino acid linker following a similar reaction condition (Scheme 4).

### Antiviral properties

Antiviral properties of compounds **5a–g**, **12a–k**, and **16** were determined against SARS-CoV-2 utilizing the standard protocol.<sup>[14,26–28]</sup> Favipiravir was used as a standard reference



**Scheme 3.** An alternate route to synthesize pyrazine-benzothiazole conjugates **12a–k** with amino acid linkers.



**Scheme 4.** Synthesis of pyrazine-benzothiazole conjugate **16**.

(positive control) for the study. Cytotoxic properties were also determined against the normal cell line VERO-E6 by the standard MTT technique to evaluate the therapeutic/selectivity index of the tested compounds. Table 1 (Figure 2) reveals that compound **5e** is superior among all the tested analogs with selectivity index 2.71 folds relative to the standard reference used (Favipiravir) due to its higher potency ( $IC_{50}$ ) against viral cells and lower cytotoxicity ( $CC_{50}$ ) against normal cells ( $IC_{50}=0.477$ , 1.382;  $CC_{50}=4.916$ , 5.262 mM for **5e** and Favipiravir, respectively). Compound **12i** also shows a similar observation ( $IC_{50}=0.3638$ ;  $CC_{50}=1.396$  mM) with slightly higher selectivity index that of Favipiravir ( $SI=3.837$ ). Compound **5f** exhibits a close therapeutic index to that of the standard reference ( $SI=3.685$ ). Although compound **5d** reveals the highest potency against SARS-CoV-2 among all the tested compounds its lower selectivity index than Favipiravir ( $IC_{50}=0.120$ ,  $CC_{50}=0.378$  mM;  $SI=3.150$ ) hindered its biological viability.

Based on the observed results, few SAR (structure-activity relationships) can be assigned. The methoxy group attached at the *para*-position of the phenyl ring at the *N*-1 of triazolyl

heterocycle seems essential for optimizing an effective antiviral agent comparable with the halogen substituent (fluorine or chlorine) as shown in compounds **5a/5b/5d**. However, an opposite rule was exhibited for the *ortho* substitution. Where the *o*-chlorophenyl containing agent is of an enhanced antiviral property than the *o*-methoxyphenyl analog and better selectivity index as exhibited in pairs **5f/5g** ( $IC_{50}=0.952$ , 1.079;  $CC_{50}=3.508$ , 2.308 mM;  $SI=3.685$ , 2.139 for **5f** and **5g**, respectively).

It has also been noticed that the unsubstituted methylene connecting the benzothiazolyl and pyrazinecarboxamide heterocycles are of higher antiviral properties relative to the substituted methylene containing-analogs as shown in compound **12a** ( $IC_{50}=0.2064$  mM). Utilization of phenylalanine for constructing pyrazine-benzothiazole conjugate afforded a potent antiviral active agent with enhanced therapeutic index than the tryptophan amino acid as shown in pairs **12i/12h** ( $IC_{50}=0.3638$ , 2.993;  $CC_{50}=1.396$ , 1.142 mM;  $SI=3.837$ , 0.382 for **12i** and **12h**, respectively).

Compounds **5a–g** have ester linkage and **12a–k** have amide linkage. Several triazole-containing bioactive molecules were reported for *in-vitro* and *in-vivo* activities in the literature

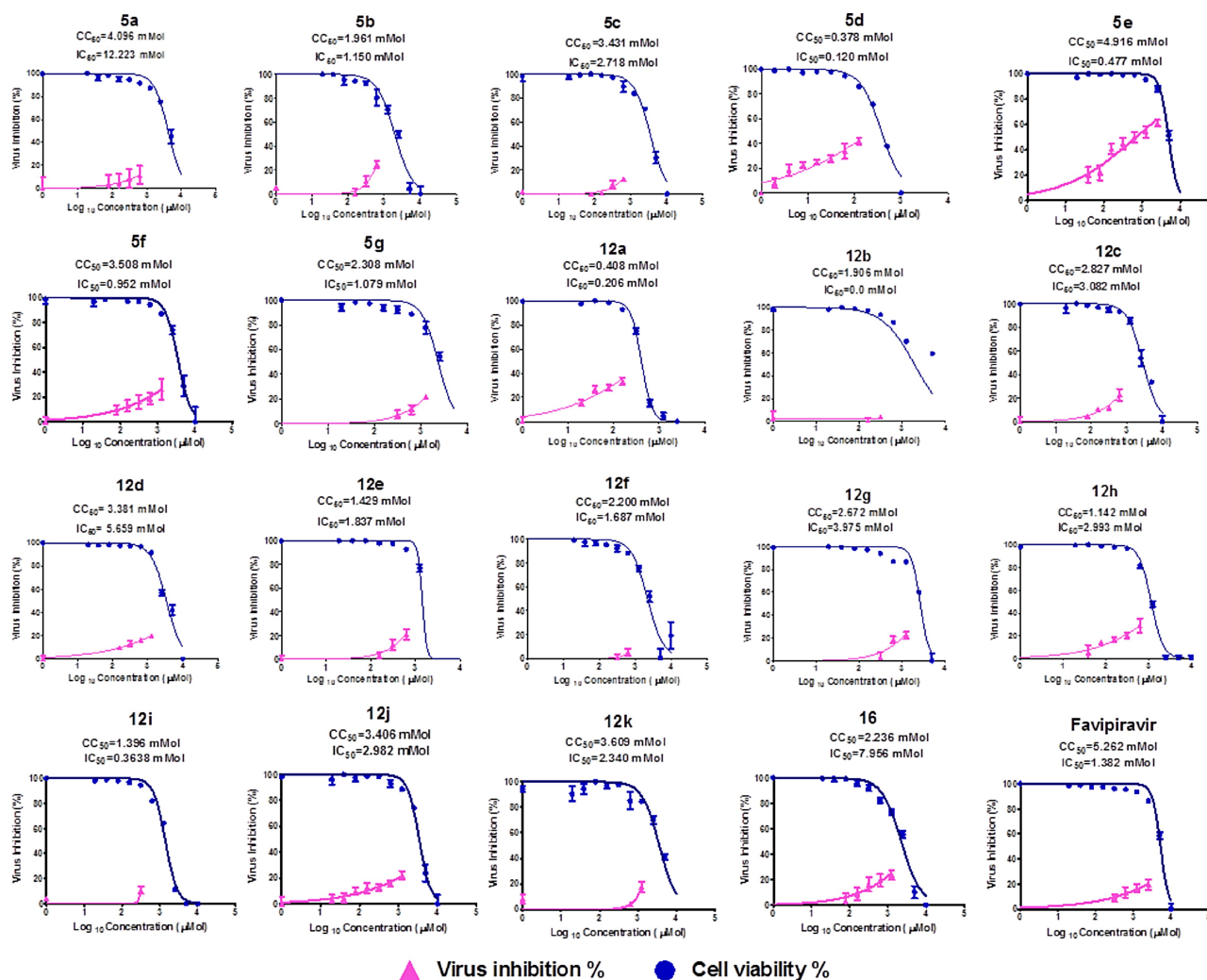
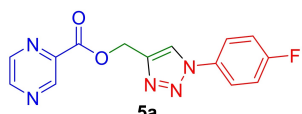
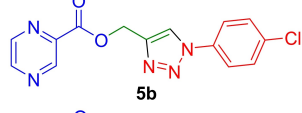
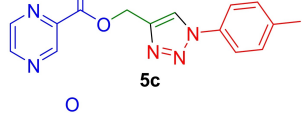
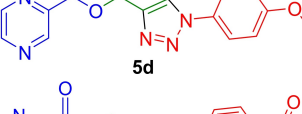
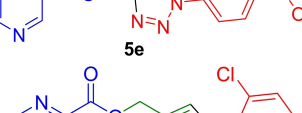
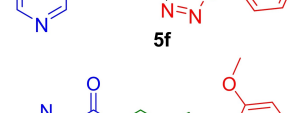
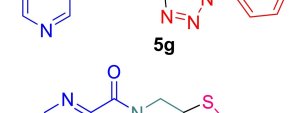
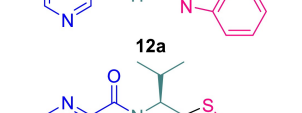
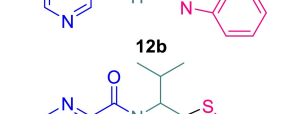
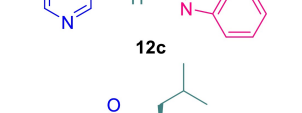
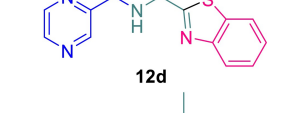
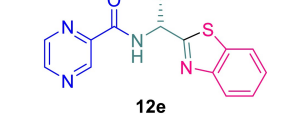
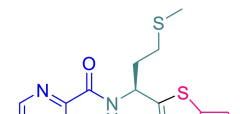
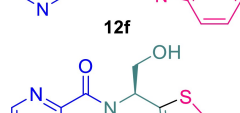
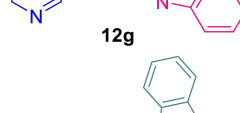
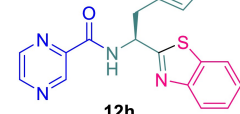
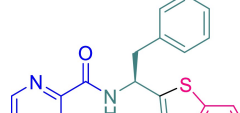
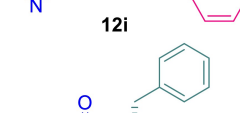
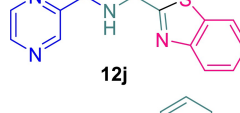
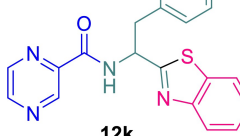


Figure 2. Dose-response curves for the tested compounds against SARS-CoV-2.

**Table 1.** Antiviral properties of the tested compounds against SARS-CoV-2.

Entry	Compd.	IC <sub>50</sub> [mM] <sup>[a]</sup>	CC <sub>50</sub> [mM] <sup>[b]</sup>	SI <sup>[c]</sup>
1	 <b>5a</b>	12.223	4.098	0.335
2	 <b>5b</b>	1.150	1.961	1.705
3	 <b>5c</b>	2.718	3.431	1.262
4	 <b>5d</b>	0.120	0.378	3.150
5	 <b>5e</b>	0.477	4.916	10.306
6	 <b>5f</b>	0.952	3.508	3.685
7	 <b>5g</b>	1.079	2.308	2.139
8	 <b>12a</b>	0.2064	0.4088	1.981
9	 <b>12b</b>	0	1.906	–
10	 <b>12c</b>	3.082	2.827	0.917
11	 <b>12d</b>	5.659	3.381	0.597
12	 <b>12e</b>	1.837	1.429	0.778

**Table 1.** continued

Entry	Compd.	IC <sub>50</sub> [mM] <sup>[a]</sup>	CC <sub>50</sub> [mM] <sup>[b]</sup>	SI <sup>[c]</sup>
13	 <b>12f</b>	1.687	2.200	1.304
14	 <b>12g</b>	3.975	3.577	0.900
15	 <b>12h</b>	2.993	1.142	0.382
16	 <b>12i</b>	0.3638	1.396	3.837
17	 <b>12j</b>	2.982	3.406	1.142
18	 <b>12k</b>	2.340	3.609	1.542
19	 <b>16</b>	7.956	2.236	0.281
20	 <b>Favipiravir</b>	1.382	5.262	3.808

[a] CC<sub>50</sub> = Concentration (cytotoxic) for the 50% cell growth of the tested agent relative to the control experiment. [b] IC<sub>50</sub> = Concentration (inhibitory) for the 50% cell growth of the tested agent relative to the control experiment. [c] SI (Selectivity index/therapeutic index) = CC<sub>50</sub>/IC<sub>50</sub>.

which are having ester linkage.<sup>[29–31]</sup> We believe our synthesized conjugates need further investigation to determine the *in-vivo* stability.

## QSAR study

QSAR is an important computational technique widely used in medicinal chemical studies for determining the parameters essential for bio-observations. It is usually used to predict/calculate the bio-properties *via* mathematical equations in terms of descriptors (physicochemical parameters).<sup>[9]</sup> Robust three descriptor model ( $R^2=0.872$ ,  $R^2cvOO=0.818$ ,  $R^2cvMO=0.783$ ) was obtained describing the antiviral properties of the tested conjugates (Supporting Information Figure S1, Tables S1–S3). The QSAR model covers a wide range of antiviral properties ( $\approx 12$  mM; due to  $IC_{50(\text{observed})}=0.120\text{--}12.223$ ,  $IC_{50(\text{predicted})}=0.227\text{--}12.137$ ).

The number of fluorine atoms is a constitutional descriptor with the highest Student *t*-criterion value among the other model's descriptors ( $t=7.627$ ) with a positive coefficient factor (8.852). This is an indication of the low antiviral properties of the compound possessing a high mathematical descriptor value. The appearance of this descriptor with a high *t*-value supports the previously mentioned SAR due to the low antiviral properties of compounds possessing *p*-fluorophenyl ring relative to the *p*-methoxyphenyl system as exhibited in pairs **5a/5d** (descriptor value = 1, 0; for **5a** and **5d**, respectively).

The maximum bond order of atom C is a semi-empirical descriptor with a negative coefficient value ( $-44.3495$ ). This is why the conjugate with a high mathematical descriptor value optimizes potent effective agent as shown in pairs **5a/5e** (descriptor value = 1.778, 1.854 corresponding to predicted  $IC_{50}=12.137$ , 0.227 mM for **5a** and **5e**, respectively). Mulliken bond orders can be calculated by Equation (1).<sup>[32]</sup>

$$P_{AB} = \sum_{i=1}^{\text{occ}} \sum_{\mu \in A} \sum_{v \in B} n_i c_{i\mu} c_{iv} \quad (1)$$

Where,  $n_i$  stands for the occupation number of the  $i_{th}$  molecular orbitals. The  $c_{i\mu}$ ,  $c_{iv}$  are the molecular orbital coefficients for the atomic orbitals  $\mu$  and  $v$ .

The HACA-1/TMSA is a charge-related descriptor that also negatively participated in the QSAR model ( $-113.9$ ). Again the higher mathematical descriptor value estimates higher antiviral potency as shown in pairs **5f** and **5g** (descriptor value = 0.01139, 0.01081 corresponding to predicted  $IC_{50}=0.439$ , 1.867 mM for **5f** and **5g**, respectively). The appearance of HACA-1 (hydrogen bonding acceptor ability) as an important descriptor controlling the observed bio-properties, also supports the attained SAR due to the role of the methoxy group relative to the halogen substituent attached to the phenyl ring at the *para*-position in enhancing the antiviral properties. The fractional hydrogen bonding acceptor ability of a molecule (FHACA-1) can be calculated by Equation (2).<sup>[32]</sup>

$$FHACA - 1 = \frac{HACA - 1}{TMSA} \quad (2)$$

Where, *HACA-1* and *TMSA* stand for the hydrogen bonding acceptor ability and total molecular surface area, respectively.

The advantage of the QSAR model achieved is supported by the estimated biological properties preserving potencies of

compounds tested among each other (Supporting Information Table S2). The statistically parameters *F* and  $s^2$  (Fisher significance and standard deviation = 29.416, 1.615, for *F* and  $s^2$  respectively) in addition to the internal validation values ( $R^2cvOO=0.818$ ,  $R^2cvMO=0.783$ ), also add good support for the QSAR model that can be utilized in a future study for predicting promising antiviral hits.

## Molecular modeling study

RdRp (RNA-dependent RNA polymerase) is an important enzyme controlling the life cycle of many viruses including coronavirus. This is due to its circular role in the transcription and replication of viral RNA. This is why the RdRp inhibitors are recognized as druggable antiviral agents.<sup>[33]</sup> Favipiravir is originally developed as an anti-Flu viral agent. Due to its RdRp inhibitory properties, it is considered for clinical trial against SARS-CoV-2.<sup>[34]</sup> The synthesized agents revealing variable anti-SARS-CoV-2 properties were considered for molecular modeling (Discovery Studio 2.5 software, standard CDOCKER technique, PDB: 7CTT) for validating the bio-observations.<sup>[35]</sup>

Compound **5d**, the most potent synthesized agent ( $IC_{50}=0.120$  mM), shows hydrogen bonding interactions with ARG555, CYS622, and LYS798 (the same amino acids revealing interactions with the co-crystallized ligand) in addition to three hydrogen bindings with LYS621 due to the pyrazinyl N and CO interactions. The  $\pi$ -cation interaction of the pyrazinyl heterocycle with the LYS798 also supports the tested agent in the protein active site affording a higher docking score relative to Favipiravir (docking score =  $-40.960$ ,  $-28.665$  kcal mol<sup>-1</sup> for **5d** and Favipiravir, respectively) (Supporting Information Figure S2).

Compounds **12a** and **12i** which are also potent anti-SARS-CoV-2 agents ( $IC_{50}=0.2064$ , 0.3638 mM for **12a** and **12i**, respectively) show hydrogen bonding with ARG555 due to the amidic CO interaction in similar behavior to Favipiravir. The additional hydrogen bonding of amidic NH with ASP760 supports the tested agents in the protein active site giving rise to the enhanced docking score values (docking score =  $-34.02$ ,  $-41.81$  for **12a** and **12i**, respectively). On the other hand, compound **5d** reveals hydrogen bonding interactions with CYS622 and LYS798, which are important amino acids of protein active site revealing interaction with the co-crystallized agent. The three hydrogen bindings of the pyrazinyl N and CO with the LYS621 enhance the docking score and explain the antiviral potency observed ( $IC_{50}=0.477$  mM, docking score =  $-42.578$  kcal mol<sup>-1</sup> for **5d**). Generally, the molecular modeling studies in the PDB: 7CTT support the observed anti-viral properties, considering that the slight divisions between the *in-vitro* antiviral and docking score values are due to the difference in the applied conditions of the experimental and computational techniques.



## ADME study

ADME (absorption, distribution, metabolism, and excretion) properties were determined by using a computational tool (Discovery Studio 2.5 software),<sup>[10]</sup> we believe these properties are important in addition to the pharmacological data. From the observed results (Supporting Information Table S4) it has been noticed that most of the tested agents show good aqueous solubility levels. Additionally, all the tested agents reveal good intestinal absorption. Plasma protein binding of all the promising synthesized antiviral agents (**5d–g** and **12i**) are at the level of 90–95%.

## Conclusion

In summary, we have designed and synthesized two sets of pyrazine-based conjugates by optimized facile reaction conditions in good yields. Some of the synthesized conjugates (**5d–g** and **12i**) showed promising antiviral properties against SARS-CoV2. The selectivity index (SI) of the potent compounds indicates significant efficacy compared to the reference drug. The preliminary antiviral studies against SARS-CoV-2 and cytotoxic data are encouraging. The computational studies adopted (QSAR and molecular modeling studies) support the observed biological properties. Calculated ADME properties are interesting and promising. The initial investigation data and computational studies could be further considered as important tools to develop new potential drug candidates for COVID-19.

## Experimental Section

Melting points were determined on a capillary tube melting point apparatus equipped with a digital thermometer Stuart SMP30 (Stuart, Cole-Parmer Instrument Co. Ltd, Staffordshire, UK). NMR spectra were recorded in CDCl<sub>3</sub> or DMSO-*d*<sub>6</sub> on a Bruker NMR spectrometer (Bruker Corporation, MA, USA) operating at 500 MHz for <sup>1</sup>H with tetramethylsilane (TMS) as an internal standard and 125 MHz for <sup>13</sup>C. HPLC high-resolution mass spectrometry (HRMS) analyses were performed on reverse phase gradient using Agilent 1200 series binary pump (G1312B; Agilent, CA, USA), waters XTerra MS C18 (3.5 μm; 2.1 × 150 mm) + Phenomenex C18 security guard column (2 × 4 mm) using 0.2% acetic acid in H<sub>2</sub>O/methanol as mobile phases; wavelength = 254 nm; and mass spectrometry was done with 6220 Agilent TOF in electrospray ionization (ESI) mode with a positive and negative method in both profile and centroid mode. HPLC studies were done with 6120 Agilent (quadrupole liquid chromatography-mass spectrometry [LC/MS]).

### Preparation of prop-2-yn-1-yl pyrazine-2-carboxylate **3**

We synthesized compound **3** by modifying a literature-reported procedure.<sup>[36]</sup> To a suspension of pyrazinoic acid **1** (1 equiv.) in *N,N*-dimethylformamide (DMF; 10 ml), K<sub>2</sub>CO<sub>3</sub> (1.4 equiv.) was added. After stirring for 30 min, propargyl bromide (1 equiv.) was added and the reaction mixture was stirred overnight. The crude mixture was diluted with water then, extracted with EtOAc (3 × 30 mL) and the combined organic layer was dried over sodium sulfate, evaporated under reduced pressure and the crude residue was purified by column chromatography.

### Preparation of pyrazinoic-triazole hybrids (**5a–g**)

To a solution of prop-2-yn-1-yl pyrazine-2-carboxylate **3** (1 mmol) in *t*-butanol/H<sub>2</sub>O (2: 1 v/v) (3 mL), CuSO<sub>4</sub> and sodium *D*-isoascorbate monohydrate was added at room temperature. To this mixture, aryl azide **4** (1.5 mmol) was added and the reaction mixture was stirred overnight. The crude mixture was diluted with water then, extracted with EtOAc (3 × 30 mL) and the combined organic layer was dried over sodium sulfate, evaporated under vacuum, and purified through column chromatography to give the pure pyrazinoic-triazole derivatives **5a–g** in good yields.

#### (1-(4-Fluorophenyl)-1H-1,2,3-triazol-4-yl)methyl pyrazine-2-carboxylate (**5a**)

White microcrystals, m.p. 130–132 °C, yield 50% (0.45 g). IR:  $\nu_{\max}$ /cm<sup>-1</sup> 3140, 2931, 1732, 1517, 1409, 1286, 992, 945, 834, 771. <sup>1</sup>H NMR (500 MHz, CDCl<sub>3</sub>)  $\delta$ : 9.32 (s, 1H), 8.76 (s, 1H), 8.71 (s, 1H), 8.15 (s, 1H), 7.67 (d, *J* = 8.4 Hz, 2H), 7.48 (d, *J* = 8.4 Hz, 2H), 5.64 (s, 2H). <sup>13</sup>C NMR (125 MHz, DMSO-*d*<sub>6</sub>)  $\delta$ : 158.8, 156.8, 143.2, 141.8, 138.3, 138.2, 128.3, 118.2, 117.9, 112.1, 111.9, 54.3. HRMS *m/z* for C<sub>14</sub>H<sub>10</sub>FN<sub>5</sub>O<sub>2</sub> [M + H]<sup>+</sup> Calcd. 300.0819. Found: 300.0821.

#### (1-(4-Chlorophenyl)-1H-1,2,3-triazol-4-yl) methyl pyrazine-2-carboxylate (**5b**)

White microcrystals, m.p. 135–138 °C, yield 36% (0.32 g). IR:  $\nu_{\max}$ /cm<sup>-1</sup> 3140, 2931, 1712, 1501, 1443, 1244, 983, 936, 825, 778. <sup>1</sup>H NMR (500 MHz, CDCl<sub>3</sub>)  $\delta$ : 9.32 (s, 1H), 8.76 (s, 1H), 8.71 (s, 1H), 8.12 (s, 1H), 7.85–7.47 (m, 2H), 7.35–6.80 (m, 2H), 5.65 (s, 2H). <sup>13</sup>C NMR (125 MHz, DMSO-*d*<sub>6</sub>)  $\delta$ : 159.1, 143.2, 141.7, 139.9, 138.3, 138.2, 130.5, 130.1, 125.3, 117.9, 117.1, 117.0, 54.3. HRMS *m/z* for: C<sub>14</sub>H<sub>10</sub>ClN<sub>5</sub>O<sub>2</sub> [M + H]<sup>+</sup> Calcd. 316.0523. Found: 316.0529.

#### (1-(*p*-Tolyl)-1H-1,2,3-triazol-4-yl) methyl pyrazine-2-carboxylate (**5c**)

White microcrystals, m.p. 112–114 °C, yield 45% (0.41 g). IR:  $\nu_{\max}$ /cm<sup>-1</sup> 3140, 2931, 1708, 1519, 1447, 1243, 938, 816, 776. <sup>1</sup>H NMR (500 MHz, CDCl<sub>3</sub>)  $\delta$ : 9.33 (s, 1H), 8.76 (s, 1H), 8.72 (s, 1H), 8.13 (s, 1H), 7.58 (d, *J* = 8.3 Hz, 2H), 7.29 (d, *J* = 8.2 Hz, 2H), 5.65 (s, 2H), 2.40 (s, 3H). <sup>13</sup>C NMR (125 MHz, CDCl<sub>3</sub>)  $\delta$ : 164.09, 148.12, 146.67, 144.78, 143.29, 142.75, 139.42, 134.75, 131.57, 130.5, 122.9, 121.0, 121.5, 59.39, 21.32. HRMS *m/z* for: C<sub>15</sub>H<sub>13</sub>N<sub>5</sub>O<sub>2</sub> [M + H]<sup>+</sup> Calcd. 296.1069. Found: 296.1073.

#### (1-(4-Methoxyphenyl)-1H-1,2,3-triazol-4-yl) methyl pyrazine-2-carboxylate (**5d**)

White microcrystals, m.p. 110–112 °C, yield 36% (0.32 g). IR:  $\nu_{\max}$ /cm<sup>-1</sup> 3140, 2931, 1722, 1518, 1409, 1255, 900, 941, 830, 774. <sup>1</sup>H NMR (500 MHz, CDCl<sub>3</sub>)  $\delta$ : 9.29 (s, 1H), 8.73 (s, 1H), 8.69 (s, 1H), 8.07 (s, 1H), 7.64–7.51 (m, 2H), 6.99–6.93 (m, 2H), 5.62 (s, 2H), 3.82 (s, 3H). <sup>13</sup>C NMR (125 MHz, CDCl<sub>3</sub>)  $\delta$ : 151.3, 148.9, 148.2, 146.7, 130.5, 126.9, 126.3, 125.7, 121.5, 112.4, 59.5, 56.2. HRMS *m/z* for: C<sub>15</sub>H<sub>13</sub>N<sub>5</sub>O<sub>3</sub> [M + H]<sup>+</sup> Calcd. 312.1018. Found: 312.1019.

#### (1-(4-Nitrophenyl)-1H-1,2,3-triazol-4-yl)methyl pyrazine-2-carboxylate (**5e**)

White microcrystals, m.p. 172–174 °C, yield 34% (0.21 g). IR:  $\nu_{\max}$ /cm<sup>-1</sup> 3145, 2931, 1710, 1505, 1415, 1299, 958, 843, 795, 758. <sup>1</sup>H NMR (500 MHz, CDCl<sub>3</sub>)  $\delta$ : 9.31 (s, 1H), 8.76 (d, *J* = 2.1 Hz, 1H), 8.71 (s, 1H), 8.40 (d, *J* = 9.0 Hz, 2H), 8.30 (s, 1H), 7.97 (d, *J* = 9.0 Hz, 2H), 5.67

(s, 2H).  $^{13}\text{C}$  NMR (125 MHz,  $\text{CDCl}_3$ )  $\delta$ : 164.1, 148.3, 147.6, 146.7, 144.8, 143.8, 143.1, 141.1, 125.8, 122.9, 120.9, 59.1. HRMS  $m/z$  for  $\text{C}_{14}\text{H}_{10}\text{N}_6\text{O}_4$   $[\text{M} + \text{H}]^+$  Calcd. 327.0764. Found: 327.0769.

#### (1-(2-Chlorophenyl)-1H-1,2,3-triazol-4-yl)methyl pyrazine-2-carboxylate (5f)

White microcrystals, m.p. 120–122 °C, yield 27% (0.24 g). IR:  $\nu_{\text{max}}/\text{cm}^{-1}$  3140, 2931, 1731, 1517, 1409, 1286, 992, 945, 834, 771.  $^1\text{H}$  NMR (500 MHz,  $\text{CDCl}_3$ )  $\delta$ : 9.29 (s, 1H), 8.73 (s, 1H), 8.69 (s, 1H), 8.16 (s, 1H), 7.74–7.47 (m, 2H), 7.48–7.29 (m, 2H), 5.65 (s, 2H).  $^{13}\text{C}$  NMR (125 MHz,  $\text{CDCl}_3$ )  $\delta$ : 163.8, 147.9, 146.4, 144.6, 143.1, 141.8, 134.6, 130.9, 130.8, 128.6, 127.9, 127.8, 126.5, 59.0. HRMS  $m/z$  for  $\text{C}_{14}\text{H}_{10}\text{ClN}_5\text{O}_2$   $[\text{M} + \text{H}]^+$  Calcd. 316.0523. Found: 316.0522.

#### (1-(2-Methoxyphenyl)-1H-1,2,3-triazol-4-yl)methyl pyrazine-2-carboxylate (5g)

White microcrystals, m.p. 101–103 °C, yield 51% (0.46 g). IR:  $\nu_{\text{max}}/\text{cm}^{-1}$  3145, 2931, 1710, 1505, 1415, 1299, 958, 843, 795, 758.  $^1\text{H}$  NMR (500 MHz,  $\text{CDCl}_3$ )  $\delta$ : 9.34 (s, 1H), 8.95–8.41 (m, 2H), 8.29 (s, 1H), 7.76 (dd,  $J=7.9, 1.5$  Hz, 1H), 7.59–7.29 (m, 1H), 7.15–6.95 (m, 2H), 5.67 (s, 2H), 3.88 (s, 3H).  $^{13}\text{C}$  NMR (125 MHz,  $\text{CDCl}_3$ )  $\delta$ : 151.3, 148.9, 148.2, 146.7, 130.5, 126.9, 126.3, 125.7, 121.5, 112.5, 59.5, 56.2. HRMS  $m/z$  for  $\text{C}_{15}\text{H}_{13}\text{N}_5\text{O}_3$   $[\text{M} + \text{H}]^+$  Calcd. 312.1018. Found: 312.1026.

#### Preparation of pyrazinoic acid-aminoacyl benzotriazolides 10a–k

1H-Benzotriazole **6** (4.0 mM) was dissolved in anhydrous methylene chloride (30 mL). Thionyl chloride (1.2 mM) was added to the solution and stirred for 30 min. Reduced the reaction mixture temperature to  $-15^\circ\text{C}$  and then the corresponding pyrazinoic acid-amino acid conjugates (**9a–k**, 1.0 mM) was added. The reaction mixture was stirred for 4–5 h at  $-15^\circ\text{C}$ . Upon completion of the reaction, the reaction mixture was filtered and the filtrate was evaporated under reduced pressure. The residue was treated with sodium carbonate solution (10%) and the precipitate obtained was filtered, washed with water, and dried to yield the desired product **10a–k**.

#### Preparation of pyrazinoic acid- benzothiazole conjugates 12a–k

A dried heavy-walled Pyrex tube containing a small stir bar was charged with benzotriazole intermediate **10a–k** (0.7 mM) and 2-aminothiophenol **11** (0.7 mM) dissolved in THF (3 mL). The reaction mixture was exposed to microwave irradiation (50 W) at a temperature of  $100^\circ\text{C}$  for 2 h. Each mixture was allowed to cool through an inbuilt system until the temperature had fallen below  $30^\circ\text{C}$  (ca. 10 min). The reaction mixture was quenched with ice-cold water and the solid obtained was filtered and washed with  $\text{Na}_2\text{CO}_3$  solution (10%) and water to give the desired compounds **12a–k**.

#### N-(Benzo[d]thiazol-2-ylmethyl)pyrazine-2-carboxamide (12a)

White microcrystals, m.p. 204–206 °C, yield 57% (0.25 g). IR:  $\nu_{\text{max}}/\text{cm}^{-1}$  3293, 3028, 2961, 1683, 1505, 1435, 899, 870, 770, 757.  $^1\text{H}$  NMR (500 MHz,  $\text{CDCl}_3$ )  $\delta$ : 10.69 (s, 1H), 9.47 (s, 1H), 8.89–8.80 (m, 1H), 8.57 (d,  $J=2.3$  Hz, 1H), 8.44 (d,  $J=9.1$  Hz, 1H), 7.48 (d,  $J=9.1$  Hz, 1H), 7.22 (t,  $J=8.5$  Hz, 1H), 6.97 (t,  $J=7.5$  Hz, 1H), 5.35 (d,  $J=6.3$  Hz, 2H).  $^{13}\text{C}$  NMR (125 MHz,  $\text{CDCl}_3$ )  $\delta$ : 167.9, 163.5, 160.8, 152.8, 147.9, 147.6, 144.7, 144.6, 144.1, 143.0, 139.5, 137.0, 135.3, 132.1,

126.5, 125.6, 124.8, 123.1, 121.9, 120.5, 115.2, 41.8. HRMS  $m/z$  for  $\text{C}_{13}\text{H}_{10}\text{N}_4\text{OS}$   $[\text{M} + \text{H}]^+$  Calcd. 270.3100. Found: 270.3101.

#### (S)-N-(1-(Benzo[d]thiazol-2-yl)-2-methylpropyl) pyrazine-2-carboxamide (12b)

White microcrystals, m.p. 215–217 °C, yield 94% (0.41 g). IR:  $\nu_{\text{max}}/\text{cm}^{-1}$  3290, 3028, 2961, 1682, 1519, 1436, 1284, 899, 871, 740.  $^1\text{H}$  NMR (500 MHz,  $\text{CDCl}_3$ )  $\delta$ : 9.37 (s, 1H), 8.76 (d,  $J=7.7$  Hz, 1H), 8.62–8.52 (m, 2H), 8.13 (s, 1H), 7.34 (d,  $J=7.1$  Hz, 1H), 7.16 (dd,  $J=7.6, 1.2$  Hz, 1H), 7.02 (t,  $J=7.6$  Hz, 1H), 6.83 (d,  $J=8.7$  Hz, 1H), 2.50–2.35 (m, 1H), 1.20 (d,  $J=6.8$  Hz, 3H), 1.05–1.00 (m, 3H).  $^{13}\text{C}$  NMR (125 MHz,  $\text{CDCl}_3$ )  $\delta$ : 164.9, 162.4, 147.8, 147.6, 144.7, 144.3, 143.0, 142.8, 135.1, 128.1, 127.4, 124.5, 119.8, 116.6, 66.1, 34.4, 17.7, 17.4. HRMS  $m/z$  for  $\text{C}_{16}\text{H}_{16}\text{N}_4\text{OS}$   $[\text{M} + \text{Na}]^+$  Calcd. 312.3910. Found: 312.3915.

#### N-(1-(Benzo[d]thiazol-2-yl)-2-methylpropyl) pyrazine-2-carboxamide (12c)

White microcrystals, m.p. 212–214 °C, yield 55% (0.24 g). IR:  $\nu_{\text{max}}/\text{cm}^{-1}$  3289, 3028, 2961, 1682, 1576, 1437, 1284, 900, 871, 740.  $^1\text{H}$  NMR (500 MHz,  $\text{CDCl}_3$ )  $\delta$ : 9.37 (s, 1H), 8.77 (d,  $J=2.4$  Hz, 1H), 8.60 (s, 1H), 8.54 (d,  $J=8.8$  Hz, 1H), 8.26 (d,  $J=8.2$  Hz, 1H), 8.14 (d,  $J=8.3$  Hz, 1H), 7.66 (t,  $J=7.7$  Hz, 1H), 7.52 (t,  $J=7.7$  Hz, 1H), 6.15 (dd,  $J=9.0, 5.1$  Hz, 1H), 2.44–2.40 (m, 1H), 1.16 (d,  $J=6.8$  Hz, 3H), 1.07 (d,  $J=6.9$  Hz, 3H).  $^{13}\text{C}$  NMR (125 MHz,  $\text{CDCl}_3$ )  $\delta$ : 164.9, 162.4, 147.8, 147.6, 144.7, 144.3, 143.0, 142.8, 135.1, 128.1, 127.4, 124.5, 119.8, 116.6, 66.1, 34.4, 17.7, 17.4. HRMS  $m/z$  for  $\text{C}_{16}\text{H}_{16}\text{N}_4\text{OS}$   $[\text{M} + \text{H}]^+$  Calcd. 312.3910. Found: 312.3911.

#### (S)-N-(1-(Benzo[d]thiazol-2-yl)-3-methylbutyl) pyrazine-2-carboxamide (12d)

White microcrystals, m.p. 219–221 °C, yield 25% (0.11 g). IR:  $\nu_{\text{max}}/\text{cm}^{-1}$  3263, 3028, 2961, 1641, 1578, 1436, 1284, 862, 741.  $^1\text{H}$  NMR (500 MHz,  $\text{CDCl}_3$ )  $\delta$ : 9.37 (s, 1H), 8.77 (d,  $J=2.4$  Hz, 1H), 8.63–8.56 (m, 1H), 8.40 (d,  $J=8.2$  Hz, 1H), 8.24 (d,  $J=8.2$  Hz, 1H), 8.13 (d,  $J=8.3$  Hz, 1H), 7.65 (t,  $J=7.7$  Hz, 1H), 7.52 (t,  $J=7.7$  Hz, 1H), 6.30–6.17 (m, 1H), 2.08–2.0 (m, 1H), 1.96–1.82 (m, 2H), 1.12 (d,  $J=6.5$  Hz, 3H), 0.99 (d,  $J=6.6$  Hz, 3H).  $^{13}\text{C}$  NMR (125 MHz,  $\text{CDCl}_3$ )  $\delta$ : 169.1, 163.3, 147.5, 144.5, 140.0, 136.3, 132.0, 126.2, 124.7, 123.7, 121.6, 58.7, 37.2, 25.1, 15.8, 11.5. HRMS  $m/z$  for  $\text{C}_{17}\text{H}_{18}\text{N}_4\text{OS}$   $[\text{M} + \text{H}]^+$  Calcd. 326.8180. Found: 326.8186.

#### N-((1S)-1-(Benzo[d]thiazol-2-yl)-2-methylbutyl) pyrazine-2-carboxamide (12e)

White microcrystals, m.p. 222–224 °C, yield 46% (0.2 g). IR:  $\nu_{\text{max}}/\text{cm}^{-1}$  3284, 3028, 2961, 1682, 1577, 1436, 1284, 899, 871, 740.  $^1\text{H}$  NMR (500 MHz,  $\text{CDCl}_3$ )  $\delta$ : 9.44 (s, 1H), 8.77 (s, 1H), 8.55 (s, 1H), 8.44 (d,  $J=8.6$  Hz, 1H), 8.30 (d,  $J=8.1$  Hz, 1H), 7.35 (t,  $J=7.8$  Hz, 1H), 7.14 (d,  $J=9.0$  Hz, 1H), 6.95 (t,  $J=7.6$  Hz, 1H), 4.57 (dd,  $J=8.6, 6.5$  Hz, 1H), 2.17–2.10 (m, 1H), 1.38–1.19 (m, 2H), 1.04 (d,  $J=6.8$  Hz, 3H), 0.96 (t,  $J=7.4$  Hz, 3H).  $^{13}\text{C}$  NMR (125 MHz,  $\text{CDCl}_3$ )  $\delta$ : 169.1, 163.3, 147.5, 144.5, 140.0, 136.3, 132.0, 126.2, 124.7, 123.7, 121.6, 58.7, 37.2, 25.1, 15.8, 11.5. HRMS  $m/z$  for  $\text{C}_{17}\text{H}_{18}\text{N}_4\text{OS}$   $[\text{M} + \text{H}]^+$  Calcd. 326.4180. Found: 326.4189.

#### (S)-N-(1-(Benzo[d]thiazol-2-yl)-3-(methylthio)propyl) pyrazine-2-carboxamide (12f)

White microcrystals, m.p. 209–211 °C, yield 82% (0.36 g). IR:  $\nu_{\text{max}}/\text{cm}^{-1}$  3314, 2931, 1660, 1516, 1415, 1299, 865, 762, 730.  $^1\text{H}$  NMR

(500 MHz, CDCl<sub>3</sub>) δ: 9.38 (s, 1H), 8.78 (d, *J* = 2.5 Hz, 1H), 8.65 (d, *J* = 8.2 Hz, 1H), 8.60 (d, *J* = 1.8 Hz, 1H), 8.25 (d, *J* = 8.2 Hz, 1H), 8.15 (d, *J* = 8.3 Hz, 1H), 7.67 (t, *J* = 7.6 Hz, 1H), 7.53 (t, *J* = 7.7 Hz, 1H), 6.30 (td, *J* = 8.5, 4.2 Hz, 1H), 2.61 (ddd, *J* = 19.8, 9.7, 4.2 Hz, 2H), 2.40–2.32 (m, 2H), 2.08 (s, 3H). <sup>13</sup>C NMR (125 MHz, CDCl<sub>3</sub>) δ: 170.9, 163.0, 153.1, 147.8, 144.8, 144.2, 142.9, 135.0, 126.5, 125.7, 123.3, 121.9, 51.2, 34.9, 30.4, 15.7. HRMS *m/z* for C<sub>16</sub>H<sub>16</sub>N<sub>4</sub>O<sub>2</sub> [M+H]<sup>+</sup> Calcd. 344.4510. Found: 344.4513.

**(S)-N-(1-(Benzo[d]thiazol-2-yl)-2-hydroxyethyl) pyrazine-2-carboxamide (12 g)**

White microcrystals, m.p. 205–207 °C, yield 25% (0.11 g). IR:  $\nu_{\max}$ /cm<sup>-1</sup> 3368, 2931, 1672, 1518, 1443, 1274, 970, 824, 798, 770, 706. <sup>1</sup>H NMR (500 MHz, CDCl<sub>3</sub>) δ: 9.39 (s, 1H), 9.18 (d, *J* = 8.3 Hz, 1H), 8.82 (d, *J* = 2.4 Hz, 1H), 8.67–8.59 (m, 1H), 8.03 (t, *J* = 8.2 Hz, 1H), 7.79 (d, *J* = 8.0 Hz, 1H), 7.62 (d, *J* = 8.3 Hz, 1H), 7.51 (t, *J* = 7.7 Hz, 1H), 5.55 (dd, *J* = 14.4, 5.9 Hz, 1H), 5.42 (dd, *J* = 14.4, 5.0 Hz, 2H), 3.50 (q, *J* = 7.0 Hz, 1H). <sup>13</sup>C NMR (125 MHz, CDCl<sub>3</sub>) δ: 167.8, 163.3, 153.0, 147.9, 145.7, 144.5, 143.0, 134.9, 133.5, 127.8, 126.5, 125.6, 124.2, 123.2, 121.8, 120.0, 109.4, 51.7, 50.7. HRMS *m/z* for C<sub>14</sub>H<sub>12</sub>N<sub>4</sub>O<sub>2</sub>S [M+H]<sup>+</sup> Calcd. 480.5394. Found: 480.5399.

**(S)-N-(1-(Benzo[d]thiazol-2-yl)-2-(1H-indol-3-yl)ethyl) pyrazine-2-carboxamide (12 h)**

White microcrystals, m.p. 255–257 °C, yield 94% (0.41 g). IR:  $\nu_{\max}$ /cm<sup>-1</sup> 3346, 2931, 1667, 1510, 843, 795, 742. <sup>1</sup>H NMR (500 MHz, CDCl<sub>3</sub>) δ: 9.36 (s, 1H), 8.71 (d, *J* = 2.0 Hz, 1H), 8.43 (s, 1H), 8.28 (d, *J* = 7.7 Hz, 1H), 8.10 (s, 1H), 7.58 (d, *J* = 8.0 Hz, 1H), 7.33 (d, *J* = 8.2 Hz, 1H), 7.21–7.12 (m, 2H), 7.10–6.97 (m, 3H), 5.13 (dd, *J* = 13.4, 5.7 Hz, 1H), 3.54–3.39 (m, 2H). <sup>13</sup>C NMR (125 MHz, CDCl<sub>3</sub>) δ: 163.4, 158.1, 147.7, 144.6, 143.0, 139.4, 136.4, 127.7, 123.2, 122.6, 120.0, 119.0, 118.1, 111.4, 110.1, 53.1, 30.0. HRMS *m/z* for C<sub>22</sub>H<sub>17</sub>N<sub>5</sub>OS [M+H]<sup>+</sup> Calcd. 340.4230. Found: 340.4240.

**(S)-N-(1-(Benzo[d]thiazol-2-yl)-2-phenylethyl) pyrazine-2-carboxamide (12 i)**

White microcrystals, m.p. 221–223 °C, yield 83% (0.40 g). IR:  $\nu_{\max}$ /cm<sup>-1</sup> 3318, 3028, 2936, 1657, 1470, 1203, 914, 886, 870, 776, 756, 708. <sup>1</sup>H NMR (500 MHz, CDCl<sub>3</sub>) δ: 9.36 (s, 1H), 8.74 (d, *J* = 2.4 Hz, 1H), 8.61 (d, *J* = 8.4 Hz, 1H), 8.56–8.50 (m, 1H), 8.04 (d, *J* = 8.2 Hz, 1H), 7.80 (d, *J* = 8.0 Hz, 1H), 7.48 (t, *J* = 8.2 Hz, 1H), 7.37 (t, *J* = 8.1 Hz, 1H), 7.29–7.10 (m, 5H), 5.87 (dd, *J* = 15.4, 6.9 Hz, 1H), 3.52 (qd, *J* = 13.9, 6.9 Hz, 2H). <sup>13</sup>C NMR (125 MHz, CDCl<sub>3</sub>) δ: 171.1, 162.7, 152.8, 147.6, 144.5, 143.9, 142.8, 136.0, 134.8, 129.5, 128.6, 127.1, 126.3, 125.4, 123.1, 121.8, 53.0, 41.4. HRMS *m/z* for: C<sub>20</sub>H<sub>16</sub>N<sub>4</sub>OS [M+H]<sup>+</sup> Calcd. 360.4350. Found: 360.4358.

**(R)-N-(1-(Benzo[d]thiazol-2-yl)-2-phenylethyl) pyrazine-2-carboxamide (12 j)**

White microcrystals, m.p. 225–227 °C, yield 62% (0.27 g). IR:  $\nu_{\max}$ /cm<sup>-1</sup> 3329, 3028, 2936, 1664, 1520, 1433, 1206, 918, 883, 860, 772, 760, 710. <sup>1</sup>H NMR (500 MHz, CDCl<sub>3</sub>) δ: 9.35 (s, 1H), 8.74 (d, *J* = 2.4 Hz, 1H), 8.67 (d, *J* = 8.3 Hz, 1H), 8.55 (d, *J* = 1.6 Hz, 1H), 8.07 (d, *J* = 8.2 Hz, 1H), 7.81 (d, *J* = 7.8 Hz, 1H), 7.53–7.46 (m, 1H), 7.39 (t, *J* = 8.1 Hz, 1H), 7.25–7.17 (m, 5H), 5.91–5.86 (m, 1H), 3.60–3.48 (m, 2H). <sup>13</sup>C NMR (125 MHz, CDCl<sub>3</sub>) δ: 171.2, 162.8, 152.9, 147.7, 144.7, 144.2, 142.9, 136.2, 134.9, 129.7, 128.8, 127.3, 126.5, 125.5, 123.3, 121.9, 53.2, 41.6. HRMS *m/z* for: C<sub>20</sub>H<sub>16</sub>N<sub>4</sub>OS [M+H]<sup>+</sup> Calcd. 360.4350. Found: 360.4362.

**N-(1-(Benzo[d]thiazol-2-yl)-2-phenylethyl) pyrazine-2-carboxamide (12 k)**

White microcrystals, m.p. 230–232 °C, yield 80% (0.35 g). IR:  $\nu_{\max}$ /cm<sup>-1</sup> 3318, 3028, 2936, 1657, 1526, 1456, 1205, 915, 885, 862, 773, 755, 710. <sup>1</sup>H NMR (500 MHz, CDCl<sub>3</sub>) δ: 9.40 (s, 1H), 8.79 (d, *J* = 1.7 Hz, 1H), 8.70 (d, *J* = 7.8 Hz, 1H), 8.59 (s, 1H), 8.10 (d, *J* = 8.2 Hz, 1H), 7.85 (d, *J* = 8.0 Hz, 1H), 7.53 (t, *J* = 7.7 Hz, 1H), 7.42 (t, *J* = 7.6 Hz, 1H), 7.31–7.18 (m, 5H), 5.93 (dd, *J* = 15.4, 7.0 Hz, 1H), 3.58–3.48 (m, 2H). <sup>13</sup>C NMR (125 MHz, CDCl<sub>3</sub>) δ: 171.2, 162.8, 152.9, 147.7, 144.7, 144.2, 142.9, 136.2, 134.9, 129.7, 128.8, 127.3, 126.5, 125.5, 123.3, 121.9, 53.2, 41.6. HRMS *m/z* for: C<sub>20</sub>H<sub>16</sub>N<sub>4</sub>OS [M+H]<sup>+</sup> Calcd. 360.4350. Found: 360.4351.

**Preparation of pyrazinoic acid- benzothiazole conjugates 16**

A dried heavy-walled Pyrex tube containing a small stir bar was charged with benzotriazole activated pyrazinoic acid **7** (0.7 mM) and 2-aminothiophenol **11** (0.7 mM) dissolved in THF (3 mL). The reaction mixture was exposed to microwave irradiation (50 W) at a temperature of 100 °C for 2 h. Each mixture was allowed to cool through an inbuilt system until the temperature had fallen below 30 °C (ca. 10 min). The reaction mixture was quenched with ice-cold water and the solid obtained was filtered and washed with Na<sub>2</sub>CO<sub>3</sub> solution (10%) and water to give the desired compound **16**.

**2-(Pyrazin-2-yl)benzo[d]thiazole (16)**

White microcrystals, m.p. 201–203 °C, yield 27% (0.12 g). IR:  $\nu_{\max}$ /cm<sup>-1</sup> 3100, 2931, 1664, 1510, 1454, 978, 851, 767, 755, 736. <sup>1</sup>H NMR (500 MHz, CDCl<sub>3</sub>) δ: 9.67 (s, 1H), 8.70 (d, *J* = 10.3 Hz, 2H), 8.18 (d, *J* = 8.2 Hz, 1H), 8.01 (d, *J* = 8.0 Hz, 1H), 7.58 (t, *J* = 7.7 Hz, 1H), 7.50 (t, *J* = 7.2 Hz, 1H). <sup>13</sup>C NMR (125 MHz, CDCl<sub>3</sub>) δ: 160.8, 147.9, 147.6, 144.7, 143.0, 139.6, 137.1, 132.1, 124.8, 120.5, 117.6. HRMS *m/z* for C<sub>11</sub>H<sub>7</sub>N<sub>3</sub>S [M+H]<sup>+</sup> Calcd. 213.2580. Found: 213.2593.

**Biological studies**

**MTT cytotoxicity assay**

To assess the half-maximal cytotoxic concentration (CC<sub>50</sub>), stock solutions of the tested compounds were prepared in 10% DMSO in ddH<sub>2</sub>O and diluted further to the working solutions with DMEM. The cytotoxic activity of the compounds was tested in VERO-E6 cells by using the 3-(4,5-dimethylthiazol-2-yl)-2,5-diphenyltetrazolium bromide (MTT) method with minor modifications. Briefly, the cells were seeded in 96 well-plates 100 μl/well at a density of 3 × 10<sup>5</sup> cell/ml and incubated for 24 h at 37 °C in 5% CO<sub>2</sub>. After 24 h, cells were treated with various concentrations of the tested compounds in triplicates. 24 h later, the supernatant was discarded and cell monolayers were washed with sterile 1 × phosphate buffer saline (PBS) 3 times, and MTT solution (20 μl of 5 mg/ml) was added to each well and incubated at 37 °C for 4 h followed by medium aspiration. In each well, the formed formazan crystals were dissolved with 200 μl of acidified isopropanol (0.04 M HCl in absolute isopropanol = 0.073 ml HCl in 50 ml isopropanol). The absorbance of formazan solutions was measured at λ<sub>max</sub> 540 nm with 620 nm as a reference wavelength using a multi-well plate reader. The percentage of cytotoxicity compared to the untreated cells was determined with the following equation.



$$\% \text{ Cytotoxicity} = \frac{\left( \frac{\text{the absorbance of cells without treatment} - \text{absorbance of cells with treatment}}{\text{the absorbance of cells without treatment}} \right) \times 100}{\text{the absorbance of cells without treatment}}$$

The plot of % cytotoxicity versus sample concentration was used to calculate the concentration which exhibited 50% cytotoxicity ( $CC_{50}$ ).<sup>[26–28,37,38]</sup>

### $IC_{50}$ determination

In 96-well tissue culture plates,  $2.4 \times 10^4$  VERO-E6 cells were distributed in each well and incubated overnight at a humidified 37 °C incubator under 5%  $CO_2$  condition. The cell monolayers were then washed with  $1 \times$  PBS and subjected to virus absorption (hCoV-19/Egypt/NRC-03/2020, Accession Number on GSAID: EPI\_ISL\_430820) for 1 h at room temperature (RT). The cell monolayers were further overlaid with 50  $\mu$ l of DMEM containing varying concentrations of the test sample, following incubation at 37 °C in 5%  $CO_2$  incubator for 72 h. The cells were fixed with 100  $\mu$ l of 4% paraformaldehyde for 20 min. and stained with 0.1% crystal violet in distilled water for 15 min. at room temperature. The crystal violet dye was then dissolved using 100  $\mu$ l absolute methanol per well and the optical density of the color is measured at 570 nm using Anthos Zenyth 200 rt plate reader (Anthos Labtec Instruments, Heerhugowaard, Netherlands). The  $IC_{50}$  of the compound is that required to reduce the virus-induced cytopathic effect (CPE) by 50%, relative to the virus control.<sup>[26–28,37,38]</sup>

### QSAR studies

The synthesized agents revealing variable antiviral properties along with Favipiravir (standard reference) were utilized for developing the 2D-QSAR modeling by CODESSA-Pro (comprehensive descriptors for structural and statistical analysis) software. Geometry of the compounds was initially optimized by AM1 technique using hyperChem 8.0 and then uploaded to CODESSA-Pro for final geometrical structure optimization by MOPAC.<sup>[8,39]</sup> CODESSA-Pro calculated 808 molecular descriptors (constitutional, topological, geometrical, charge-related, semi-empirical, thermodynamic, molecular-type, atomic-type and bond-type descriptors) for the exported agents. Mathematical transformation of the experimental values (including  $IC_{50}$ ,  $1/IC_{50}$ ,  $\log(IC_{50})$  and  $1/\log(IC_{50})$  mM) were used searching for the best QSAR model. The best multi-linear regression (BMLR) technique was utilized which is a stepwise search for the best  $n$ -parameter regression equations (where  $n$  stands for the number of descriptors used), based on the highest  $R^2$  (squared correlation coefficient),  $R^2_{cvOO}$  (squared cross-validation “leave one-out, LOO” coefficient),  $R^2_{cvMO}$  (squared cross-validation “leave many-out up to 20% of the training set, LMO” coefficient),  $F$  (Fisher statistical significance criteria) values, and  $s^2$  (standard deviation). The QSAR up to 3-descriptor model describing the biological activity of the antiviral active agents were generated (obeying the thumb rule of 5.7:1 which is the ratio between the data points and the number of QSAR descriptors).

### Acknowledgements

We thank the Egyptian Cultural and Educational Bureau Scholarship. The authors also thank the Center for Undergraduate Research and Scholarship (CURS), Translational Research Program

(TRP) at Augusta University, and the Egyptian Academy of Scientific Research and Technology (ASRT, Ideation Fund program, contract number 7303) for the financial support.

### Conflict of Interest

The authors declare no conflict of interest

**Keywords:** Pyrazine · 1,2,3-Triazole · Benzothiazole · SARS-CoV-2 · Computational studies

- [1] H. Lu, C. W. Stratton, Y.-W. Tang, *J. Med. Virol.* **2020**, *92*, 401–402.
- [2] Q. Li, X. Guan, P. Wu, X. Wang, L. Zhou, Y. Tong, R. Ren, K. S. M. Leung, E. H. Y. Lau, J. Y. Wong, X. Xing, N. Xiang, Y. Wu, C. Li, Q. Chen, D. Li, T. Liu, J. Zhao, M. Liu, W. Tu, C. Chen, L. Jin, R. Yang, Q. Wang, S. Zhou, R. Wang, H. Liu, Y. Luo, Y. Liu, G. Shao, H. Li, Z. Tao, Y. Yang, Z. Deng, B. Liu, Z. Ma, Y. Zhang, G. Shi, T. T. Y. Lam, J. T. Wu, G. F. Gao, B. J. Cowling, B. Yang, G. M. Leung, Z. Feng, *N. Engl. J. Med.* **2020**, *382*, 1199–1207.
- [3] N. Chen, M. Zhou, X. Dong, J. Qu, F. Gong, Y. Han, Y. Qiu, J. Wang, Y. Liu, Y. Wei, J. Xia, T. Yu, X. Zhang, L. Zhang, *Lancet* **2020**, *395*, 507–513.
- [4] World Health Organization, 2020. Clinical management of severe acute respiratory infection when novel coronavirus (nCoV) infection is suspected: interim guidance, (<https://www.who.int/emergencies/diseases/novel-coronavirus-2019/technical-guidance-publications>).
- [5] G. Ursinia, G. Punzia, B. W. Langworthyc, Q. Chena, K. Xiad, E. A. Cornead, B. D. Goldman, M. A. Stynerg, R. C. Knickmeyerj, J. H. Gilmored, D. R. Weinberger, *Proc. Natl. Acad. Sci. USA* **2021**, *118*, e2021946118.
- [6] B. B. Gowen, M.-H. Wong, K.-H. Jung, D. F. Smee, J. D. Morrey, Y. Furuta, *Antiviral Res.* **2010**, *86*, 121–127.
- [7] Search of: favipiravir|Covid19 – list results – clinicaltrials.gov. 2020. <https://clinicaltrials.gov/ct2/results?cond=Covid19&term=favipiravir&cntry=&state=&city=&dist=Clinicaltrials.gov>. [online] Available at: <https://clinicaltrials.gov/ct2/results?cond=Covid19&term=favipiravir&cntry=&state=&city=&dist=Clinicaltrials.gov>.
- [8] S. S. Panda, A. S. Girgis, H. H. Honkanadavar, R. F. George, A. M. Srour, *Future Med. Chem.* **2020**, *12*, 1369–1386.
- [9] S. S. Panda, A. S. Girgis, S. J. Thomas, J. E. Capito, R. F. George, A. Salman, M. A. El-Manawaty, A. Samir, *Eur. J. Med. Chem.* **2020**, *196*, 112293.
- [10] I. A. Seliem, S. S. Panda, A. S. Girgis, Y. I. Nagy, R. F. George, W. Fayad, N. G. Fawzy, T. S. Ibrahim, A. M. M. Al-Mahmoudy, R. Sakhujia, Z. K. M. Abdel-samii, *Chem. Biol. Drug Des.* **2020**, *95*, 248–259.
- [11] S. S. Panda, A. S. Girgis, B. B. Mishra, M. Elagawany, V. Devarapalli, W. F. Littlefield, A. Samir, N. G. Fawzy, A. M. Srour, *RSC Adv.* **2019**, *9*, 20450–20462.
- [12] H. M. Faidallah, A. S. Girgis, A. D. Tiwari, H. H. Honkanadavar, S. J. Thomas, A. Samir, A. Kalmouch, K. A. Alamry, K. A. Khan, T. S. Ibrahim, A. M. M. Al-Mahmoudy, A. M. Asiri, S. S. Panda, *Eur. J. Med. Chem.* **2018**, *143*, 1524–1534.
- [13] H. M. Faidallah, S. S. Panda, J. C. Serrano, A. S. Girgis, K. A. Khan, K. A. Alamry, T. Therathanakorn, M. J. Meyers, F. M. Sverdrup, C. S. Eickhoff, S. G. Getchell, A. R. Katritzky, *Bioorg. Med. Chem.* **2016**, *24*, 3527–3539.
- [14] I. A. Seliem, S. S. Panda, A. S. Girgis, Y. Moatasim, A. Kandeil, A. Mostafa, M. A. Ali, E. S. Nossier, F. Rasslan, A. M. Srour, R. Sakhujia, T. S. Ibrahim, Z. K. M. Abdel-samii, A. M. M. Al-Mahmoudy, *Bioorg. Chem.* **2021**, *114*, 105117.
- [15] B. Zhang, *Eur. J. Med. Chem.* **2019**, *44*, 357–372.
- [16] D. K. Kim, J. Kim, H. J. Park, *Bioorg. Med. Chem. Lett.* **2004**, *14*, 2401–2405.
- [17] M. Whiting, J. C. Tripp, Y.-C. Lin, W. Lindstrom, A. J. Olson, J. H. Elder, K. B. Sharpless, V. V. Fokin, *J. Med. Chem.* **2006**, *49*, 7697–7710.
- [18] Z.-Y. Cheng, W.-J. Li, F. He, J.-M. Zhou, X.-F. Zhu, *Bioorg. Med. Chem.* **2007**, *15*, 1533–1538.
- [19] F. d C. da Silva, M. C. B. V. de Souza, I. I. P. Frugulhetti, H. C. Castro, S. L. d O Souza, T. M. L. de Souza, D. Q. Rodrigues, A. M. T. Souza, P. A. Abreu, F. Passamani, C. R. Rodrigues, V. F. Ferreira, *Eur. J. Med. Chem.* **2009**, *44*, 373–383.
- [20] C. G. Mortimer, G. Wells, J.-P. Crochard, E. L. Stone, T. D. Bradshaw, M. F. G. Stevens, A. D. Westwell, *J. Med. Chem.* **2006**, *49*, 179–185.
- [21] G. Akhilesh, R. Swati, *J. Chem. Pharm. Res.* **2010**, *2*, 244–258.
- [22] S. Bondock, W. Fadaly, M. Metwally, *Eur. J. Med. Chem.* **2010**, *45*, 3692–3701.

- [23] J. Neres, M. L. Brewer, L. Ratier, H. Botti, A. Buschiazzo, P. N. Edwards, P. N. Mortenson, M. H. Charlton, P. M. Alzari, A. C. Frasc, R. A. Bryce, K. T. Douglas, *Bioorg. Med. Chem. Lett.* **2009**, *19*, 589–596.
- [24] A. Rana, N. Siddiqui, S. A. Khan, S. E. Haque, M. A. Bhat, *Eur. J. Med. Chem.* **2008**, *43*, 1114–1122.
- [25] P. J. Palmer, R. B. Trigg, J. V. Warrington, *J. Med. Chem.* **1971**, *14*, 248–251.
- [26] M. Feoktistova, P. Geserick, M. Leverkus, *Cold Spring Harb Protoc.* **2016**, doi:10.1101/pdb.prot087379.
- [27] A. Mostafa, A. Kandeil, Y. A. M. M. Elshaier, O. Kutkat, Y. Moatasim, A. A. Rashad, M. Shehata, M. R. Goma, N. Mahrous, S. H. Mahmoud, M. GabAllah, H. Abbas, A. El Taweel, A. E. Kayed, M. N. Kamel, M. El Sayes, D. B. Mahmoud, R. El-Shesheny, G. Kayali, M. A. Ali, *Pharmaceuticals* **2020**, *13*, 443.
- [28] R. Alnajjar, A. Mostafa, A. Kandeil, A. A. Al-Karmalawy, *Heliyon* **2020**, *6*, e05641.
- [29] D. T. G. Gonzaga, L. B. G. Ferreira, T. E. M. M. Costa, N. L. von Ranke, P. A. F. Pacheco, A. P. S. Simoes, J. C. Arruda, L. P. Dantas, H. Rezend de Freitas, R. A. Reis, C. Penido, M. L. Bello, H. C. Castro, C. R. Rodrigues, V. F. Ferreira, R. X. Faria, F. de Carvalho da Silva, *Eur. J. Med. Chem.* **2017**, *139*, 698–717.
- [30] R. I. Filho, D. T. G. Gonzaga, T. M. Demaria, J. G. B. Leandro, D. C. S. Costa, V. F. Ferreira, M. C. Sola-Penna, F. C. da Silva, P. Zancan, *Curr. Top. Med. Chem.* **2018**, *18*, 1483–1493.
- [31] D. Kumar, K. Beena, G. Khare, S. Kidwai, A. K. Tyagi, R. Singh, D. S. Rawat, *Eur. J. Med. Chem.* **2014**, *81*, 301–313.
- [32] A. R. Katritzky, R. Petrukhin, I. Petrukina, A. Lomaka, D. B. Tatham, M. Karelson, **2005**. CODESSA-Pro software manual pp. 67, 70.
- [33] D. Kumar, G. Chauhan, S. Kalra, B. Kumar, M. S. Gill, *Bioorg. Chem.* **2020**, *104*, 104326.
- [34] Shagufta, I. Ahmad, *Eur. J. Med. Chem.* **2021**, *213*, 113157.
- [35] <https://www.rcsb.org/structure/7CTT>.
- [36] R. Reddyrajulaa, U. Dalimba, *Bioorg. Med. Chem. Lett.* **2020**, *30*, 126846.
- [37] H. Yan, G. Xiao, J. Zhang, Y. Hu, F. Yuan, D. K. Cole, C. Zheng, G. F. Gao, *J. Med. Virol.* **2004**, *73*, 323–331.
- [38] N. S. Ogando, T. J. Dalebout, J. C. Zevenhoven-Dobbe, R. W. A. L. Limpens, Y. van der Meer, L. Caly, J. Druce, J. J. C. de Vries, M. Kikkert, M. Barcena, *J. Gen. Virol.* **2020**, *101*, 925–940.
- [39] R. M. Bokhtia S S Panda, A. S. Girgis, H. Honkanadavar, T. S. Ibrahim, A. M. M. Al-Mahmoudy, R. F. George, M. T. Kashef, W. Fayad, R. Sakhuja, E. H. Abdel-Aal, *Med. Chem.* **2021**, *17*, 71–84.

---

Manuscript received: July 6, 2021

Revised manuscript received: July 30, 2021

Accepted manuscript online: August 5, 2021

Version of record online: September 6, 2021